Laser and Particle Beams (1996), *vol.* 14, *no.* 2, *pp.* 211-223
Printed in the United States of America

Optical smoothing for shock-wave generation: Application to the measurement of equations of state

By DIMITRI BATANI,* SIMONE BOSSI,* ALESSANDRA BENUZZI,* MICHEL KOENIG,** BERNARD FARAL,** JEAN MICHEL BOUDENNE,** NICOLAS GRANDJOUAN,† STEFANO ATZENI,†† AND MAURO TEMPORAL††

*Dipartimento di Fisica, Università degli Studi di Milano Via Celoria 16, 20133 Milano, Italy
**Laboratoire pour l'Utilisation des Lasers Intenses Ecole Polytechnique, 91128 Palaiseau, France
†Laboratoire de Physique des Milieux Ionises Ecole Polytechnique, 91128 Palaiseau, France
††Associazione EURATOM-ENEA sulla Fusione, C.R.E Frascati, C.P. 65, 00044 Frascati, Rome, Italy
††INFN, Laboratori Nazionali di Legnaro, Via Romea 4, 35020 Legnaro, Italy

(Received 25 February 1995; accepted 28 August 1995)

Experimental results are presented on shock-wave generation in solid samples, irradiated directly by optically smoothed laser beams. Random phase plates and phased zone plates have been successfully used. In particular, the last technique allowed the production of uniform shock fronts that have been used for equation of state experiments at pressures above 10 Mbar. Pressures higher than 35 Mbar were achieved in gold, by using laser pulses with energy $E \approx 100$ J, and structured, two-step, two-material targets.

1. Introduction

The study of shock-wave dynamics plays an important role in several branches of physics, including inertial confinement fusion (ICF) (Nuckolls *et al.* 1972), and astrophysics (Ross & Nellis 1982). Moreover, the generation of high pressures (P of the order of some tens of Mbar to one Gbar) allows states of matter in extreme conditions of density and temperature to be reached. Hence, the equation of state (EOS) and properties of matter in such conditions can be studied (Eliezer *et al.* 1986; Hall *et al.* 1989; More 1991).

High-pressure shock waves have been produced using chemical (Elias *et al.* 1991) or nuclear explosions (Ragan *et al.* 1982). In the latter case, pressures in the tens of Mbar domain were achieved. Even higher pressures can, however, be achieved in the laboratory by using powerful pulsed lasers.

Early experiments (Trainor *et al.* 1978; Fabbro *et al.* 1986) clearly demonstrated that pressures up to about 100 Mbar could be obtained, but with a rather poor and uncontrolled shock quality. Indeed, one of the main problems in laser-generated shock experiments is inherent to the use of coherent laser light that results in lack of uniformity in the irradiation due to beam modulations by interference effects. Such nonuniform illumination, in turn, causes strong pressure nonuniformities that, in the past, have prevented the use of lasers as a quantitative tool in high-pressure physics. Two methods can be used to avoid such a problem and to obtain "high-quality" shock waves.

The first one is based on the conversion of coherent laser light into incoherent soft X-rays inside a laser heated cavity (hohlraum). Thin foil targets are then uniformly irradiated by

 0263-0346/96 $11.00 + .10

the exposition to the intense soft X-ray Planck radiation emitted from such a cavity. Recently, this approach, with the use of the colliding foil technique and of 25-kJ laser pulses, has allowed estimated pressures of about 0.75 Gbar to be obtained (Cauble *et al.* 1993). In this case anyway, the authors do not discuss in detail the quality of the produced shocks. In another experiment performed at the MPQ Institute in Garching (Lower *et al.* 1994), the shock quality was carefully checked even if much lower pressures were obtained (these were in the range of 10 Mbar using single Al foils as targets). In general, the drawbacks of the indirect approach are its low efficiency, due to the intermediate step of X-ray conversion, and an important induced X-ray preheating of the shocked target.

The second method, which constitutes the main subject of this article, is based on the use of the direct-drive approach with optically smoothed laser beams. This results in better laser–target coupling and in a lower X-ray preheating effect.

Our first results have been obtained using the well-known technique of random phase plates (RPP) (Kato *et al.* 1984). With RPPs we could achieve a good control of laser energy deposition and obtain reproducible series of significant results on shock dynamics. Anyway, flat shock fronts cannot be produced with RPPs, unless large focal spots and hence high laser energies are used (which is not feasible with our laser parameters). To overcome such a difficulty we adopted the new technique of phased zone plates (PZP) (Stevenson *et al.* 1994), which allows the production of flat-top intensity distributions of laser light in the focal spot, and hence of flat shocks. Such shock fronts make comparisons with 1D theoretical models and computer simulations much easier. Therefore, accurate studies on shock dynamics and EOS experiments can be performed with the use of direct laser drive and moderate laser energy.

Generally, EOS experiments require two parameters of the compressed matter (such as shock velocity, fluid velocity, shock temperature, etc.) to be measured independently (Zel'dovich & Raizer 1966). Indeed Hugoniot and shock relations represent a set of equations that allows the determination of one EOS point once two shock-related quantities have been measured. In a recent experiment (Hammel *et al.* 1993), the shock velocity and the fluid velocity have been determined together on the same laser shot. However, such an experiment requires implementing sophisticated diagnostics; moreover, very high power lasers are required to obtain a large focal spot and to maintain a constant ablation pressure for a time long enough (a few nanoseconds, as imposed by diagnostics resolution). In our experiments, instead, we adopted a scheme based on the use of "two step-two material" targets and the impedance-matching technique (Zel'dovich & Raizer 1966), which allows relative measurements of the EOS of an unknown material with respect to a known "reference" material. Preliminary experiments using the same principle were performed in the past (Holmes *et al.* 1982) with bigger laser facilities, but at lower pressures (below 10 Mbar) and, above all, with larger experimental errors (uncertainties in shock speed determination about 10%). Instead, using a 100-J laser, we have been able to produce shocks with pressures as high as 35 Mbar, and to measure shock speed with uncertainty $\approx 5\%$.

2. Experimental set-up

The experiments have been performed at the Laboratoire pour l'Utilisation des Lasers Intenses (LULI) Laboratory, Ecole Polytechnique, and some preliminary results have been presented in Koenig *et al.* (1994). They were based on the detection of the emissivity of the target rear face (opposite to the laser beams) in the visible region. A photographic objective imaged the rear face onto the slit of a visible streak camera to record the variations in time of this emission. The system magnification was $M = 22$, allowing a ≈ 5-μm spatial resolution, which was measured imaging a suitable grid. We note that according to diffrac-

tion theory, the elementary speckles produced by either RPPs or PZPs are smaller than the quoted resolution, and hence cannot be directly evidenced in experimental results.

The experiments have been performed with three of the six LULI laser beams (converted in second harmonic, $\lambda = 0.53$ μm, with total laser energy $E_{2\omega} \leq 100$ J) focused onto the same focal spot. The temporal behavior of the laser pulse was Gaussian with $t_L = 600$ ps (FWHM). A fourth beam, also converted to 2ω, was used as a temporal fiducial. Each beam had a $\Phi = 90$-mm diameter and was focused on target with an $f = 50$ cm lens (figure 1).

An equivalent plane diagnostic was implemented for controlling the laser focal spot. The system was based on an imaging objective (Olympus 50 mm, 1/1.2, the same used to image the target rear side onto the streak camera slit) and a charge-coupled-device (CCD) camera (12 bits, 512 × 512 pixels). A removable mirror allowed the image to be directed to either the CCD or to the streak camera , so that we had an almost "on-line" control of the focal spot shape, which could be easily checked between two shots.

Finally, an active X-ray pinhole camera, looking at the target on the laser side, at 22.5° with respect to the laser beams plane, was used to check plasma formation and to image the focal spot in the X-ray domain, because we verified the good correspondence (shape and dimensions) with the far-field image. All the diagnostics were connected to a numeric acquisition system through a customer developed LabView software (National Instruments®) installed on an Apple® computer.

3. Measurements with RPPs and simple targets

In the first set of experiment, the beams were optically smoothed with RPPs. A large and homogeneous Gaussian focal spot ($W_s \geq 100$ μm) was produced to reduce 2D effects, giving an intensity on target $I_L \leq 2 \times 10^{14}$ W/cm^2. More precisely, the intensity was given by

$$I(r,t) = I_o \exp(-2.77\ r^2/W_s^2)\exp(-2.77\ t^2/t_L^2),$$

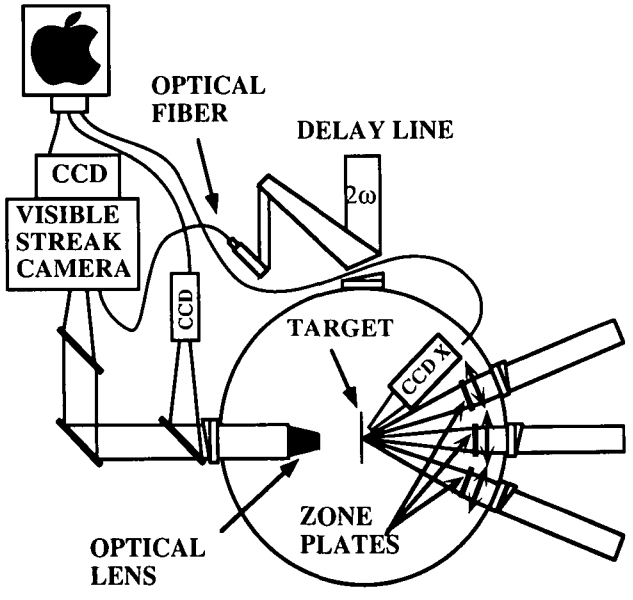

FIGURE 1. Experimental set-up.

where integrating over space and time we find the laser pulse energy $E_{2\omega}$ and see that $I_o = 0.84\, E_{2\omega}/t_L W_s^2$. Figure 2 shows a typical streak camera image obtained with an 18-μm Al target on the streak camera time-scale of 200 ps/mm. The shape of the image clearly follows the Gaussian focal spot shape. Such a shape is "shot by shot" reproducible, with no evidence of localized earlier shock breakthroughs, due to laser hot spots.

In figure 3 we plot the shock arrival time at the rear face versus the target thickness, obtained using one laser beam only. In this case we have mainly worked at two experimental laser intensities ($I_o = 2.2 \times 10^{14}$ W/cm^2 and $I_o = 1.8 \times 10^{14}$ W/cm^2). As obvious, one can see that shock arrival time is shorter for higher energies and thinner targets. Shock velocities can be obtained by interpolating these data. We found velocities of the order of $D \approx 29 \pm 3$ μm/ns for the high-intensities set of data and $D \approx 26 \pm 3$ μm/ns for the low-intensities one. The velocities were obtained by limiting the experimental data to large thicknesses ($d > 8$ μm). Indeed, with a temporally Gaussian laser pulse, there is a build-up time needed for the shock wave to reach a constant velocity.

We compared these experimental results with simulations performed with the 1D hydrodynamic Lagrangian code FILM developed at the Ecole Polytechnique. The two series of data are well reproduced, for large thicknesses, by simulations with laser intensities $I_o = 10^{14}$ W/cm^2 and $I_o = 1.5 \times 10^{14}$ W/cm^2, respectively. This applies to the shock arrival time and the shock velocity, which from simulations are 25.5 and 28.3 μm/ns, respectively. Again, data obtained from the simulations (figure 3) show the build-up phase before the shock wave reaches a constant velocity.

The differences between the experimental intensities on target and computer simulations intensities are due to different causes, including incomplete absorption of laser light and refraction of laser light in the plasma corona. Indeed, as measured in various experiments (e.g., Labaune *et al.* 1982) at our laser wavelength and intensity range, absorption efficiency should be $\approx$80%. As far as refraction is concerned, simulations performed with the 2D hydrodynamic Lagrangian code DUED developed at ENEA (Atzeni 1986, 1989) allow us to evaluate that $\leq$5% of the pulse energy is refracted away from the focal spot.

Figure 3 shows a non-negligible scattering of data for a fixed target thickness. Before discussing the measurement errors, we note that these data were obtained in three different sets of experiments with slightly modified laser parameters, including RPP design, focus-

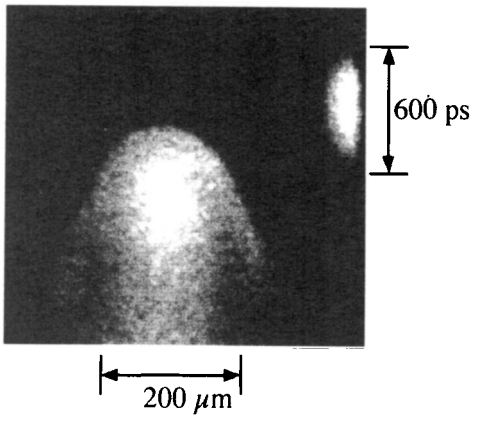

FIGURE 2. Rear side shock breakthrough for an 18-μm Al target. Optical smoothing is realized with RPPs, giving a measured focal spot diameter FWHM = 106 μm. Time fiducial is on the right of the image.

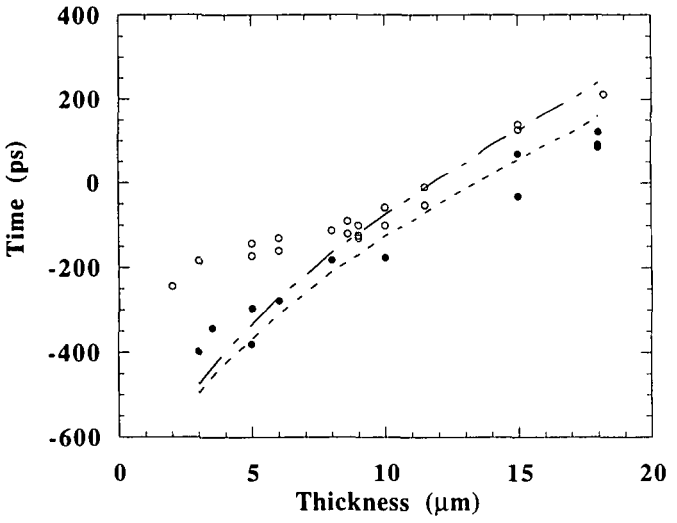

FIGURE 3. Shock breakthrough time as a function of target thickness obtained with RPPs using simple Al targets. The two curves correspond to 1D simulations performed with the lagrangian code FILM at $I_o = 1.5 \times 10^{14}$ W/cm^2 (– – –) and $I_o = 10^{14}$ W/cm^2 (—— – ——).

ing length, laser pulse duration and focal spot dimension. Now, to assess precision and reproducibility of our data, we analyze the expected experimental errors. The main sources of scattering of experimental data are errors in the measurement of the target thickness (we used here foils produced by Goodfellow with typical indetermination of the order of ±3%), the fluctuations of the laser energy around the mean values (which in our case was of the order of ±10%) and errors in the measure of the energy itself (±5%).

If the pressure is constant, the breakthrough time is a linear function of the foil thickness. Therefore, the relative error on the thickness induces a relative error on the time, which are related by

$$\sigma_t = \sigma_d / D.$$

Taking into account that the pressure is not constant from shot to shot, we have :

$$\sigma_t^2 = [(\sigma_d)^2 + (\sigma_I d/3I)^2]/D^2$$

Here $\sigma_I/I \approx \sigma_E/E$ and the factor 3 in the second term on the right-hand side comes from the dependence of the shock velocity on laser intensity, which is classically given by $D \approx I^{1/3}$ (Fabbro 1982) (different models will give a close dependence and then almost the same numerical factor). From this formula, for a 20-μm target, we get $\sigma_t \approx \pm 40$ ps. This is in good agreement with the scattering of experimental results for the high intensity (1.5×10^{14} W/cm^2). For the lower intensity, the lack of agreement is mainly due to larger errors in the measure of the laser energy.

For thin targets, for which shock velocity is not constant, the experimental shock breakthrough time shows an important discrepancy with simulations. In this case, preheating due to hard X-rays (which were not included in our simulations) plays a non-negligible role. Also, for these thicknesses, the shock is far from stationary (shock breakthrough occurs several hundred ps before pulse maximum); in addition, the emissivity of the rear face is low (the temperature being typically of the order of 1 eV) and we are then in the limit of the sensitivity of the diagnostic.

Finally, we must also note that for thick and thin targets we have another possible source of error. Due to the specific shape of the focal spot (Gaussian), the time of shock breakthrough must be detected by looking at a small area of the target rear face (in principle point-like), which corresponds to the maximum intensity in the spatial profile of the laser focal spot. This may lead to errors in the detection of shock arrival time connected to the fixed spatial resolution and to the sensitivity of the streak camera. This problem may be particularly important for thin targets, for which the rear side temperature, and hence the luminosity, are smaller at shock breakthrough.

This situation is illustrated in figure 4, which shows a simulation, performed with DUED, of the propagation of a shock wave produced by laser irradiation with a peak intensity of $I_o = 1.5 \times 10^{14}$ W/cm^2 on an 18-μm Al target. The first picture (t = 320 after the laser pulse peak) shows the arrival of the shock wave at the target rear face in the center of the focal spot; here we note that due to the Gaussian shape, laser intensity is lower at the focal spot edges and the shock wave is travelling with smaller speed. The second picture shows the situation after 80 ps where breakthrough occurs at points corresponding to $I_o/2$. At this time, in the regions where the shock wave has already arrived, the rear face is expanding backward.

4. Measurements with PZPs and simple targets

As shown in the previous section, the use of RPPs allowed a good control of laser energy deposition and of data reproducibility. Anyway the nonflat shock shape only allowed for the measurement of the shock breakthrough time and could not be used for EOS experiments. To produce flat shock fronts we adopted the new optical smoothing technique of PZPs (Stevenson *et al.* 1994). The PZPs are made of an array of Fresnel lenses, each one

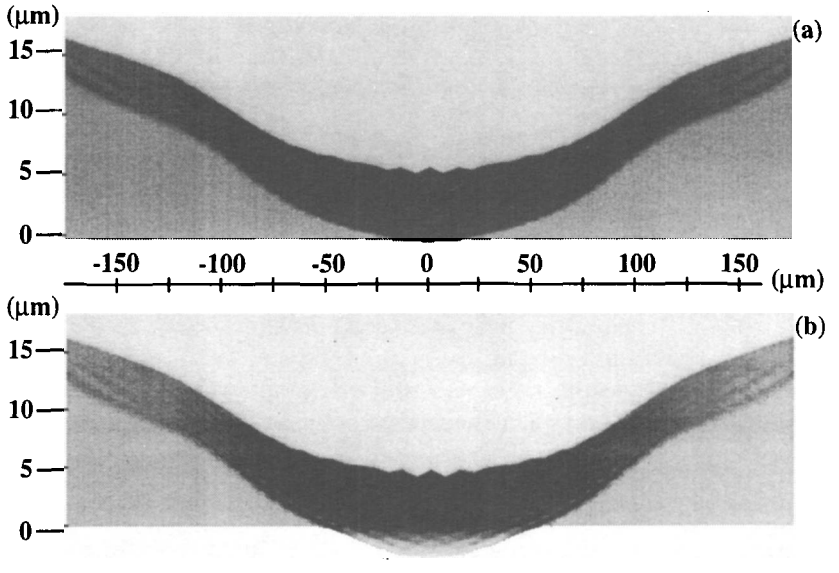

FIGURE 4. Simulation performed with the 2D hydrodynamic lagrangian code DUED. Shock propagation produced by a laser irradiation with intensity $I_o = 1.5\ 10^{14}$ W/cm^2 in a 18-μm Al target. (a) time of the shock breakthrough at the maximum intensity I_o and (b) time of the shock breakthrough at the radial positions corresponding to intensity $I = I_o/2$.

randomly introducing a phase shift (0 or π). A uniform distribution of the laser intensity is produced at a given distance from the geometrical focal point of the main focusing lens.

In our experiment the best position gave a measured focal spot composed of a $\approx$180-μm top-hat intensity distribution, with Gaussian edges (figure 5). In the resulting focal spot, a lot of small spikes are superimposed to the flat top profile due to the usual diffraction effects. The FWHM diameter of the focal spot is $\approx$400 μm, corresponding to a laser intensity $I \leq 10^{14}$ W/cm^2. Three laser beams were used to ensure similar intensity to the RPP case.

Figure 6 shows a "flat" shock breakthrough obtained using the PZPs and a simple 14-μm Al target. In this sample shock breakthrough times across a $\approx$180-μm diameter have $\Delta t = \pm 5$ ps, which is in good agreement with the focal spot size given in figure 5. Also, from a densitometry of the streak camera images as a function of time (figure 7), we see that the rear side luminosity is characterized by a steep rise, followed by a long decay. As observed by Lower *et al.* (1994), this behavior is typical of shock luminosity when preheating is negligible (i.e., when no preshock signal is present). Anyway, while in Lower's indirect drive experiments only relatively thick targets ($d \geq 17$ μm) were free of such a preheating (caused by the hard primary X rays coming from the cavity), for us this behavior is also found for much thinner targets.

By using PZPs and carefully checking laser energy and target thickness, we repeated the experiment of figure 3 and obtained more reproducible results (figure 8), allowing for the use of a 100-ps/mm time scale and for achieving a $\approx$5-ps time resolution (working with a 100-μm slit on the streak camera). The better reproducibility of the results is also due to the fact that now, unlike with the RPPs, the shock is arriving nearly simultaneously over a large region of the target rear face, which reduces the errors in the breakthrough time detection.

In concluding, we must note that, even if we have been able to produce high-quality shock waves (Koenig *et al.* 1994), our experimental conditions were not optimal for the application of the PZP technique, due to the long focal length of the focusing lens ($f = 50$ cm) on one hand, and the small beam diameter (90 mm) on the other. Hence, our results imply that even higher quality shock waves could be produced using the larger beams provided by other existing laser facilities.

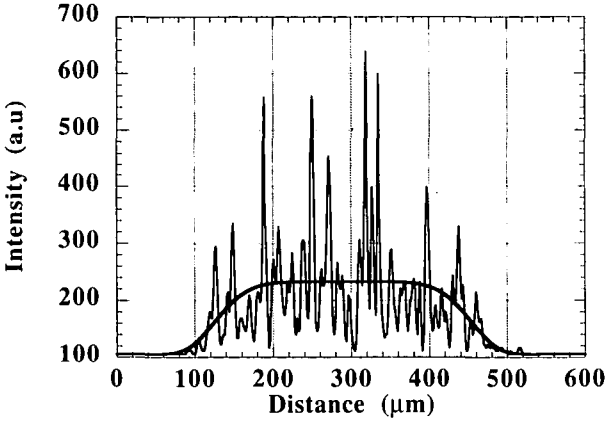

FIGURE 5. Spatial intensity profile in the focal spot produced by PZP. The solid line represents a supergaussian interpolation with a top-hat profile of $\approx$ 180 μm and FWHM of $\approx$ 400 μm.

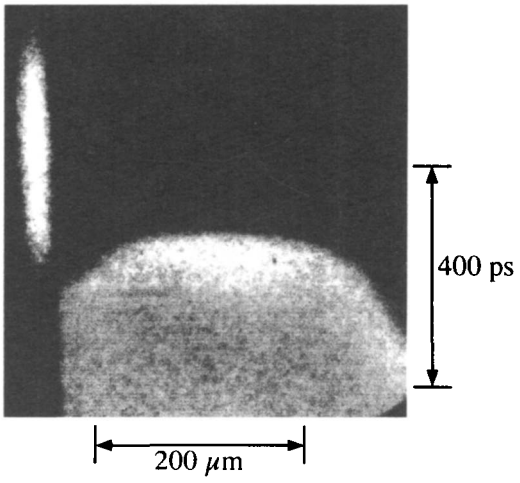

FIGURE 6. Rear-side shock breakthrough for a 14-μm Al target obtained with PZPs. Time fiducial is on the left of the image.

5. Measurements with PZPs and stepped targets

Simple foil targets allow mainly for measurements of the shock breakthrough time, and the shock velocity must be deduced by comparing results obtained under the same conditions for targets with different thickness. Anyway, also due to laser energy fluctuations, this method is time-consuming and not sufficiently accurate. For instance, as seen in section 3, the interpolated D values for the 1.5×10^{14} W/cm^2 and 1.0×10^{14} W/cm^2 cases lie within the experimental error bars.

A direct "shot-by-shot" measurement of shock velocity instead can be performed with stepped or wedged targets (Cottet *et al.* 1985). Of course, this method can only be used if 1) shock pressure is uniform on the two sides of the step and 2) shock pressure, and hence shock velocity, are constant when travelling through the step. The first point again shows the importance of producing uniform shock fronts, as those which may be produced with

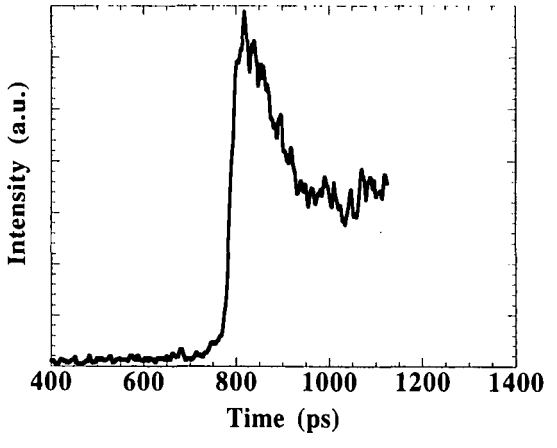

FIGURE 7. Densitometry of the streak image in figure 6 (signal as a function of time).

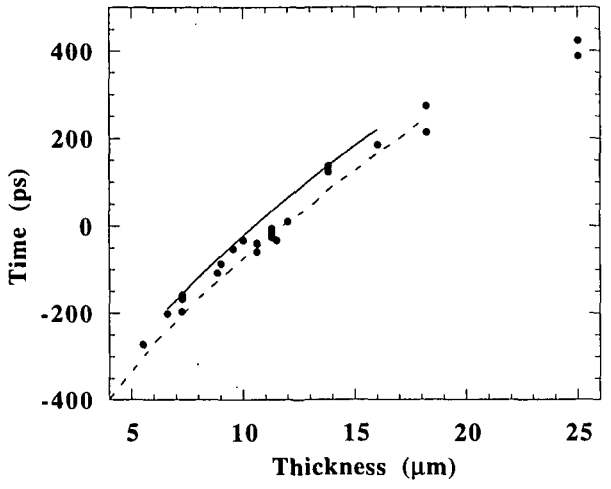

FIGURE 8. Shock breakthrough time as a function of target thickness obtained using PZPs and simple Al targets. The two curves correspond to 1D simulations performed with the lagrangian code FILM; $I_o = 8 \times 10^{13}$ W/cm^2 (solid line) $I_o = 10^{14}$ W/cm^2 (dashed line).

PZPs. Indeed, in the case of stepped targets, the Gaussian distribution produced with the "classical" RPPs would entail an increase of uncertainties on the results of measures due to the variations of the shock velocity across the focal spot. The second point may instead impose some limits on target thickness, related to the laser system performance. As already shown in figure 3, FILM simulations show that, with our laser and target parameters, a nearly constant shock velocity is obtained for targets with thickness $d \geq 8$ μm. The curve of figure 3 deviates again from the linear slope for large thicknesses. Outside this region, because the measured velocity is a mean velocity, the proposed method does not offer all its advantages.

Figure 9 shows a shock breakthrough obtained with PZPs and a stepped target. Shock velocities, measured with simple (figure 8) and stepped targets (figure 9) have now a typi-

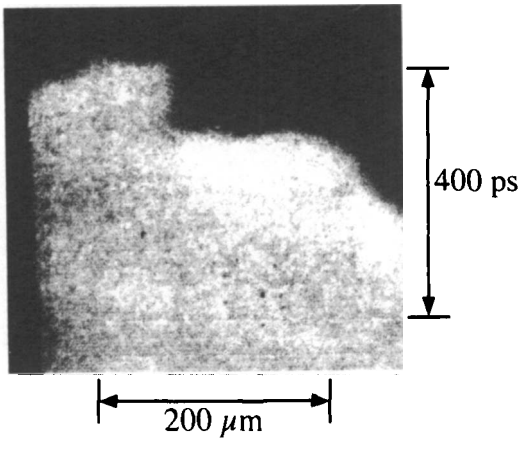

FIGURE 9. Rear-side shock breakthrough for an Al target with a 7.5-μm base and a 2.8-μm step. The measured shock velocity is $D = 24$ μm/ns.

cal value $D \approx 24$ μm/ns. We note that the lower velocity, when compared to our RPP experiment, is due to the lower intensity. By using the SESAME EOS tables (Bennett *et al.* 1978; Holian 1984), we found that these velocities correspond to pressures $P \approx 10$ Mbar in Al (Koenig *et al.* 1994).

To evaluate the precision in the measurement of the shock velocity with this technique, we consider that $D = d/t$, where d is the step thickness and t the difference between shock breakthrough times at the end of the step and at the base. For instance, for the case shown in figure 9, we have $d = 2.8$ μm and $t = 120$ ps. Then, by considering the errors on time ($\Delta t \leq 5$ ps due to shock flatness) and on the step thickness (0.05 μm), we get a shock velocity error smaller than ±4.5%. By improving shock uniformity and by using thicker steps, such an error could easily be reduced to ≤2%.

6. Double step targets: EOS measurements

6.1. *Principle of the experiment*

This experiment was based on the well-known impedance-matching technique applied to double step targets (Holmes *et al.* 1982), whose basic principle is schematically presented in figure 10. The target is made of a simple "base" foil made of material A, which supports two steps made, respectively of the same material A, and of a different material B.

If the EOS of the two materials are known, for example by SESAME (Bennett *et al.* 1978) or QEOS (More *et al.* 1988), so are their polars of shock, and it is then possible to test the relative consistency of such tables in the following way. Assume, for instance, that material B has the higher density, in which case its polar curve is located above that for material A. When the shock arrives at the interface between the two materials, a shock wave is transmitted though the material B and another one is reflected in the material A. Exper-

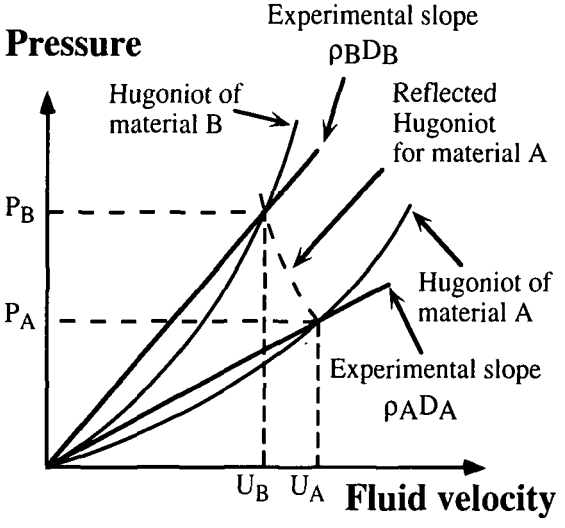

FIGURE 10. Principle of the impedance-matching experiment. The pressure and the particle velocity being continuous at the interface, the point (P_B, U_B) is located at the intersection of the Hugoniot curve of material B, issued from the initial state ($P = 0$, $U = 0$), with the curve of reflected shocks of material A, issued from the state (P_A, U_A).

imentally, we determine the two shock velocities D_A and D_B (figure 10). The lines $P_A = u\rho_A D_A$ and $P_B = u\rho_B D_B$ plotted in the (P, u) plane, intersect the Hugoniot curves in the points (P_A, u_A) and (P_B, u_B). Now, according to the laws of shock dynamics, the interface between the two media is an equilibrium surface for particle velocities and pressures; therefore, the equilibrium pressure, after the shock passage through the interface, is found by the intersection of the curve of the reflected shocks issued from (P_A, u_A) and the polar curve of material B at a point (P'_B, u'_B). Obviously if the two material tables are mutually consistent, the deduced values of pressure and shock velocity must be equal, that is, $(P'_B, u'_B) = (P_B, u_B)$.

This method can also be used to get EOS points of the second material, if the EOS of the material A is well known. Hence, materials for which there are important uncertainties, or lack of data, can be studied relatively to a well-known "reference" material (Zel'dovich *et al.* 1966).

6.2. *Target fabrication*

To perform experiments of this kind, high-quality targets are needed. Our targets have been produced in collaboration with the "Laboratoire des Cibles" of the Centre d'Etudes de Limeil-Valenton (Faral *et al.* 1994). The main constraint, apart from the good knowledge of the thickness (0.05 μm in our case), is the fact that the step needs to be sharp to minimize the experimental errors when measuring the shock velocity. With this goal, we developed a simple mechanical device in which 1) first the material of the base is deposited; and 2) a mask is applied to realize the step with another deposition.

For the two step-two material targets, a last stage followed in which a second mask was mechanically and optically guided to ensure that the steps do not overlap and that their separation is limited to more than 50 μm. The second material (gold) was then deposited. The spacing between the steps indeed must be small enough compared to the flat region of the focal spot, so that the shock generated on both steps has the same strength. The overall quality of these targets has then been checked with an electron microscope.

6.3. *Experimental results*

We performed a preliminary EOS consistency experiment (Koenig *et al.* 1995) using targets made of aluminum and gold, as materials A and B, respectively. In figure 11 we show a typical streak image of a two-step target. Here we can clearly determine the shock velocities in the two materials, the flat part of the focal spot being $\approx$200 μm, while the spacing between the two steps is $\approx$45 μm.

Due to experimental uncertainties, the aluminium shock velocity (corresponding to $P \approx$ 10 Mbar) determines a "region" on its polar curve and hence a "region" on the gold polar curve. Because this region overlaps with that obtained with the Au shock velocity, we can say that the two EOSs we used for Al and Au are consistent around $P \approx 10$ Mbar. This is not a surprise, being that both Au and Al are well-known materials in this pressure range, but it shows that this method may indeed be used for actual EOS measurements, especially because a better accuracy level can be easily reached in further developments.

Finally, in figure 12 we report a series of results we obtained on Au-Al targets. Here the shock velocity in gold D_{Au} is plotted as a function of the aluminium shock velocity D_{Al}. The corresponding pressures range from 4.5 to 16.5 Mbar in aluminum and from 9.5 to 37 Mbar in gold, depending on the input laser energy. The data (with errors bars of $\pm$4.5% and $\pm$6% for aluminium and gold, respectively) are in good agreement with the SESAME EOS (solid line).

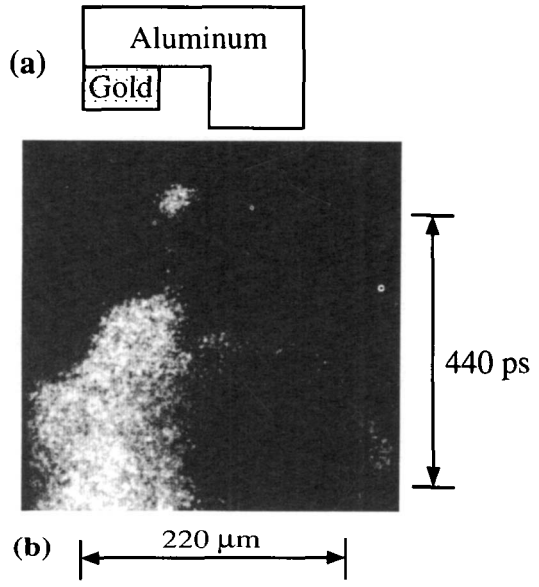

FIGURE 11. Rear-side shock breakthrough for a double step target. (a) sketch of the target; the aluminum base thickness is 9.5 μm, the steps of aluminum and gold are 4.25 μm and 1.85 μm, respectively. (b) streak camera record of visible light emitted by the rear side of the target.

7. Conclusion

These experiments have shown the possibility of obtaining reproducible and quantitative measurements on shock-wave generation and dynamics by using direct sample irradiation, with optically smoothed laser beams. By the use of PZPs, which allows the production of high-quality, uniform shock fronts, we have shown that stepped targets allow direct measurements of shock velocity and the two-step technique may be used to check EOS consis-

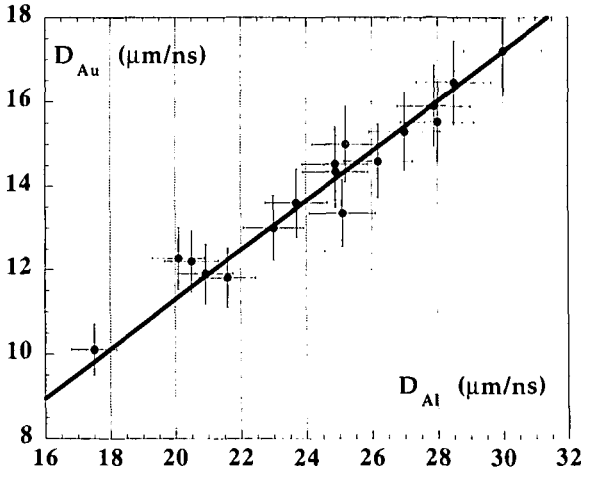

FIGURE 12. Experiments with the aluminum-gold targets. The shock velocity in gold, D_{Au}, is plotted versus the shock velocity in aluminum D_{Al}. Error bars are 4.5% and 6% for aluminum and gold, respectively. The solid line represents theoretical SESAME data.

tency. In addition, this method can be applied to get relative EOS points of a material assuming a reference EOS for another material (for example aluminium). This will be, for example, the case in future ICF experiments, in which pellets will have ablator layers made with sophisticated materials, for which EOS calculations must be experimentally checked.

Acknowledgments

This work has been supported by the "Dense Plasma and Laser Compression Physics" network in the framework of the "Human Capital and Mobility" Programme (E.U. contract No. CHRX-CT93-0338) and by the "Access to Large Facilities" Programme (E.U. contract CHGE-CT-930046). In particular, the authors thank I. Ross and C. Danson for the realization of the PZPs used in the experiment and for the useful discussions, the "Laboratoire des Cibles" of the CEA in Limeil, and Prof. E. Sindoni for his kind interest in this research. Mauro Temporal was partly supported by a SIF-ENEA fellowship and Alessandra Benuzzi by an ERASMUS grant.

REFERENCES

ATZENI, S. 1986 *Comput. Phys. Comm.* **43**, 107.

ATZENI, S. 1989 *Plasma Phys. Control. Fusion.* **31**, 2187.

BENNETT, B.I. *et al.* 1978 LANL Report LA-7130 (unpublished).

CAUBLE, R. *et al.* 1993 *Phys. Rev. Lett.* **70**, 2102.

COTTET, F. *et al.* 1985 *Appl. Phys. Lett.* **47**, 678.

ELIAS, P. *et al.* 1991 In *The Physics of Compressible Turbulent Mixing, 3rd Int. Workshop* (France).

ELIEZER, S. *et al.* 1986 *Equations of State* (Cambridge University Press, Cambridge).

FABBRO, R. 1982 *Etude de l'influence de la longuer d'onde laser sur les processus de conduction thermique et d'ablation dans les plasmas crees par laser.* These de doctorat, Université de Paris Sud-Orsay.

FABBRO, R. *et al.* 1986 *Laser Part. Beams* **4**, 413.

FARAL, B. *et al.* 1994 in Rapport Scientifique LULI 1993, 309.

HALL, T. *et al.* 1989 *Plasma Physics* **31**, 111.

HAMMEL, B.A. *et al.* 1993 *Phys. Fluids* **B5**, 2259.

HOLIAN, K.S. 1984 (ed.). Los Alamos National Laboratory Report LA-10160-MS, UC-34 (unpublished).

HOLMES, N.C. *et al.* 1982 *Shock Waves in Condensed Matter-1981*, W.J. Nellis, I. Seaman, and R.A. Graham, eds. (American Institute of Physics, New York).

KATO, Y. *et al.* 1984 *Phys. Rev. Lett.* **53**, 1057.

KOENIG, M. *et al.* 1994 *Phys. Rev. E* **50**, R3314.

KOENIG, M. *et al.* 1995 *Phys. Rev. Lett.* **74**, 2260.

LABAUNE, C. *et al.* 1982 *Phys. Rev. Lett.* **48**, 1018.

LOWER, TH. *et al.* 1994 *Phys. Rev. Lett.* **72**, 3186.

MORE, R.M. *et al.* 1988 *Phys. of Fluids* **31**, 3059.

MORE, R.M. 1991 *Physics of Laser Plasmas*, A. Rubenchik, and S. Witkowsky, eds. (North Holland, Amsterdam).

NUCKOLLS, J. *et al.* 1972 *Nature* **239**, 139.

RAGAN, C.E. *et al.* 1982 *Shock Waves in Condensed Matter-1981* W.J. Nellis, I. Seaman, and R.A. Graham, eds. (American Institute of Physics, New York).

ROSS, M. & NELLIS, W.J. 1982 *Shock Waves in Condensed Matter-1981* W.J. Nellis, I. Seaman, and R.A. Graham, eds. (American Institute of Physics, New York).

STEVENSON, R.M. *et al.* 1994 *Optics Letters* **19**, 363.

TRAINOR, R.J. *et al.* 1978 *Phys. Rev. Lett.* **42**, 1154.

ZEL'DOVICH, YA.B. & RAIZER, YU.P. 1966 *Physics of Shock Waves and High Temperature Hydrodynamic Phenomena* (Academic Press, New York).